FLING EFFECTS FROM NEAR-SOURCE STRONG MOTION RECORDS: INSIGHTS FROM THE M 6.5, 2016, NORCIA EARTHQUAKE (CENTRAL ITALY)

D'Amico M., Felicetta C., Schiappapietra E., Pacor F., Gallovic F., Paolucci R., Puglia R., Lanzano G., Sgobba S. and Luzi L.

Abstract

1. Introduction

When an earthquake occurs, the elastic strain gradually accumulated for long time on either side of a fault is suddenly released. The elastic rebound generates the dynamic component of the motion and the static deformation of the ground. In the proximity of the source of large earthquakes, this tectonic displacement may be recorded by accelerometric instruments. The corresponding waveforms have characteristic shapes, producing a one-sided pulse in the velocity trace and an offset (fling-step) at the end of the displacement waveform (Figure 1a). The fling-step may be on the order of tens or hundreds of centimeters (Boore and Bommer 2005) and it is typically observed along the slip direction: it appears along strike-parallel direction for strike-slip faults (Kalkan et al., 2004), whereas it can be observed both in the strike-normal and vertical directions for dip-slip faults (Mavroeidis and Papageorgiou, 2002; Bray and Rodriguez-Marek, 2004; Somerville 2005).

Waveforms affected by fling-step (also called permanent displacement) are of great interest in structural engineering. Reliable evaluation of the seismic displacement and, in particular, the relative displacement between contiguous points, is of key importance for extended structures or pipelines (i.e. ports, viaducts, base-isolated buildings, long-span bridges) design or assessment in order to account for the spatial variability of the near-source ground motion (Somerville 2002; Kalkan and Kunnath 2006; Akkar and Boore 2009; Kamai et al., 2014). However, the identification

of fling-containing time series is not straightforward since earthquake waveforms are far from the exact representation of the ground motion. Different sources of noise at high and low frequencies, and non-standard errors such as spurious spikes, early termination coda or multiple baselines, can mask and distort the true ground-motion (Boore and Bommer 2005; Puglia et al., 2018).

The accurate recovery of flings is difficult, in particular, due to the presence of baseline offsets that, even though small in acceleration, result in artificial long period drifts of the ground displacement (Boore et al., 2002; Graves 2004; Wang et al., 2011). The long period distortion of the signal may be caused by numerous sources, which include not only instrumental effects, such as electrical or mechanical hysteretic behaviour of the transducer, but also electronic noise, distortions due to A/D converter and ground rotation and tilting (Boore et al., 2002; Chen and Loh 2007; Wang et al., 2011).

Currently, most of the engineering processing tools for accelerometric data remove the low frequency content of the signal (e.g. Puglia et al. 2018, http://esm.mi.ingv.it/processing/; PEER, Pacific Earthquake Engineering Research, http://ngawest2.berkeley.edu/), leading to biased estimates of the ground displacement. Therefore, it is advisable to adopt alternative methods that preserve the long period spectral content related to the tectonic fling.

Many studies on the recovering permanent displacements from strong motion data, especially after the development of the modern digital recording have been published since 1970s (Wu and Wu 2007 and references therein). Noteworthy principal approaches based on simple correction of the signal baseline are Graizer (1979), Iwan et al. (1985), Boore (2001), Graves (2004), Wu and Wu (2007), Chen and Loh (2007), Chao et al. (2010), and Wang et al. (2011). However, it should be noted that any baseline adjustment can be based only on approximate and empirical methods, because of the difficulty in discerning the origin of the drifts (Boore et al., 2002; Boore and Bommer 2005). Furthermore, a still open problem among the above-mentioned methods is an objective estimation of uncertainties of the static displacements retrieved from the strong-motion records (Wang et al., 2011). In fact, different baseline correction schemes may provide different

results, as the seismic displacement is one of the most sensitive ground-motion characteristics to the adopted processing technique (Boore 2001).

The comparison with geodetic measurements or ground motion simulations may be very helpful to obtain reliable displacement traces (Burks and Baker 2016). Generally, geodetic measurements provide accurate estimates of ground displacement and studies on earthquake sources have started to widely exploit these space-geodetic methods, such as GPS (Global Positioning System) and InSAR (Interferometric Synthetic Aperture Radar). Nevertheless, these measurements are rarely available close to accelerometric stations and only a few recording stations have GPS and accelerometer sensors co-located. Ground motion simulations, which include specific features of rupture process, seismic waves propagation, and site effects, directly model both the dynamic and the static component of the fling-step. Hence, they can be useful to verify the evidence of the static displacement when observations are not available.

The scarcity of predictive models for static offset reflects the difficulty in recovering the permanent displacement from strong motion data. Nowadays, in fact, there are very few published models for fling parameters, such as those by Abrahamson (2002), Kamai et al. (2014) and Burks and Baker (2016), which are largely derived from ground-motion simulations based on strike-slip and reverse faulting scenarios.

In this work, we have developed a semi-automatic scheme, eBASCO (extended BASeline COrrection), for piecewise baseline correction of near-source records, following the approach proposed by Wu and Wu (2007) and later improved by Chao et al. (2010).

The method has been applied to reconstruct the ground displacement field of the Mw 6.5 30th October 2016 earthquake (Central Italy) and the robustness of the results has been checked using geodetic measurements (Avallone et al., 2016, ring.gm.ingv.it; De Guidi et al., 2017) and ground motion simulations (Pizzi et al., 2017) as benchmarks.

The final aim of this work is to develop a robust procedure to recover the permanent displacement that could be, e.g., fully integrated into processing web-interfaces (e.g. esm.mi.ingv.it/processing,

Puglia et al., 2018) linked to strong-motion databases. The advantage consists in making available different approaches to process strong-motion data and disseminating waveforms that exhibit fling-step for engineering purposes and seismological studies.

2. Baseline correction scheme

We propose an automatic scheme for an extended BASe-line COrrection (eBASCO), suitable to process near-source records, based on the method proposed by Wu and Wu (2007) and later improved by Chao et al. (2010). In the ideal case, acceleration waveforms are unaffected by baseline shift, so that velocity and displacement time series can be directly obtained by integration of the acceleration waveforms. Hence, the pre- and post-event velocity should oscillate around zero and the displacement trace should tend to a constant residual value, taking the shape of a smooth ramp function (Figure 1a). Conversely, in the real case, acceleration waveforms are spoiled by distortions and shifts of the base-line that results in artificial features of the velocity and displacement waveforms after the single and double integrations of the accelerations (Figure 1b).

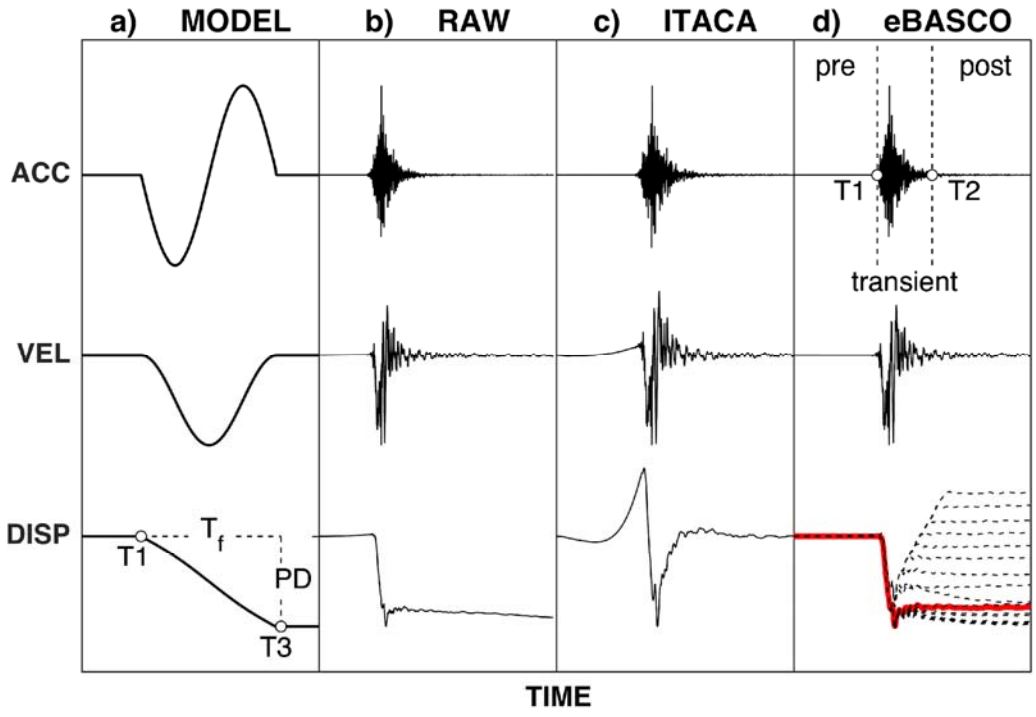

Figure 1. (a) Analytical model of the fling-step and acceleration waveform (E-W component) recorded at the station T1214 during the M_W 6.5 30th October 2016 earthquake. Middle and bottom panel represent the velocity and displacement time histories after integration of the acceleration record. (b) Uncorrected acceleration time history, and the same datum corrected by band-pass filter following (c) Puglia et al. (2018) or (d) the present piecewise linear de-trend. Pre-event, transient and post-event windows are highlighted by their limits set at T_1 and T_2. T_3 represents the time at which the ground displacement reaches the final offset. T_f and PD are the period of the sine pulse and the amplitude of the permanent displacement, respectively. Red line: eBASCO ground displacement corresponding to the optimal choice of T_1 and T_2 time correction points (maximum f-value); dashed black lines: solution set corresponding to different combinations of T_1 and T_2 correction points.

2.1 Piecewise linear de-trend

The eBASCO processing is based on a baseline adjustment of the strong-motion waveforms by means of piecewise linear de-trend. The baseline shift of an acceleration record is subdivided into three contributions (Figure 1d) defined by the following time windows: 1) pre-event window between the time of the first sample T_0 and the time T_1 from which the ground starts moving towards the permanent displacement; 2) transient window, between time points T_1 and T_2, during the strong-ground shaking; 3) post-event window from T_2 to the end of the signal.

We subtract from the acceleration trace the amplitude of the first sample. This causes that the first amplitude of the velocity waveform equals zero. The pre-event baseline V_i is firstly removed by subtracting a regression line that crosses the origin from the velocity time series. The baseline is computed as follows:

$$(\ ) = \qquad [1]$$

where A_i is the slope of the line fitting the velocity waveform in the pre-event time window.

A further least squares fitting is used to remove the linear trend in the post-event window of the velocity waveforms:

$$(\ ) = \ _{0,} + \qquad [2]$$

where A_f is the slope of the line fitting the post-event window velocity.

Following Boore (2001), a baseline offset A_m, that is representative of the complex shift in baseline during the strong shaking, is removed in the acceleration transient windows. The correction term A_m is defined satisfying the condition for which the velocity, at the end of the strong shaking, averages

to zero after the baseline correction. In order to fulfil this requirement, the velocity of the baseline correction at the end of the transient window should be equal to the velocity obtained from the fitted line $V_f(T_2)$ (Equation 2).

$$= \quad (\ _2)/(\ _2 - \ _1) \qquad [3]$$

The corrected transient-window acceleration is integrated to obtain the corresponding velocity. The pre-event, transient and post-event windows are then combined into corrected velocity waveform. Finally, the corrected displacement and acceleration traces are computed by integration and derivation of the corrected velocity time series, respectively (Figure 1d). In order to avoid unphysical jumps in the final acceleration trace, the amplitudes in T_1 and T_2 times must respect a tolerance level, such as 25% of the peak ground acceleration (PGA) as considered in the present application.

2.2 Selection of time correction points

The selection of time T_1 and T_2 plays a key role in retrieving the final permanent displacement. In fact, the procedure makes the final displacement offset very sensitive to the choice of these correction points. Although there are not specific rules to set these two times, some guidelines have been proposed in literature (Iwan et al., 1985; Boore 2001; Graves 2004). Therefore, in the absence of any objective criterion to choose the correction points, the obtained final displacement could converge toward a non-unique solution with very large variability both in terms of sign and amplitude (dashed black lines in Figure 1d). In order to reduce the degree of subjectivity in the choice of T_1 and T_2, eBASCO applies a procedure to find the optimal combination of the two correction points as follows.

- Following Chao et al. (2010) T_1 is set on the basis of the ratio of energy distribution in acceleration accumulated since the P-wave arrival. As T_1 has the physical meaning of the time at which the ground starts moving (Figure 1a), we set five different values of the time

point T_1 sampled before the 5% of the energy distribution (logarithmically spaced between 0.0001% and 5%).

- Following Wu and Wu (2007), another correction point T_3 is considered, representing the time at which the ground has just reached the permanent deformation (Figure 1a). A set of five linearly spaced time points T_3 is sampled within the last 50% of the energy distribution (Chao et al. 2010).
- After that, we evaluate the corrected displacement waveforms for all the time points T_1 and T_3 combinations; the baseline correction, described by Equations 1-3, is performed by sampling 20 logarithmically spaced time points T_2 between T_3 and the end of the signal.
- To guarantee that the corrected displacement series is flat after T_3, a flatness indicator f is defined considering the displacement trace between T_3 and the end of the signal:

$$= \frac{}{| \ |\cdot} \qquad [4]$$

where r is the linear correlation coefficient, b is the slope of the linear fit and σ is the variance of the residual displacement. Note that the displacement waveform is the flatter, the more the absolute value of r and b tends to 1 and 0, respectively, and the value of σ gets smaller.

- At the end, we consider as "best solution" the corrected displacement trace characterized by the maximum f value over all combinations of the T_1, T_2 and T_3 time points (red line in Figure 1d). The flowchart of the eBASCO procedure is shown in Figure 2.

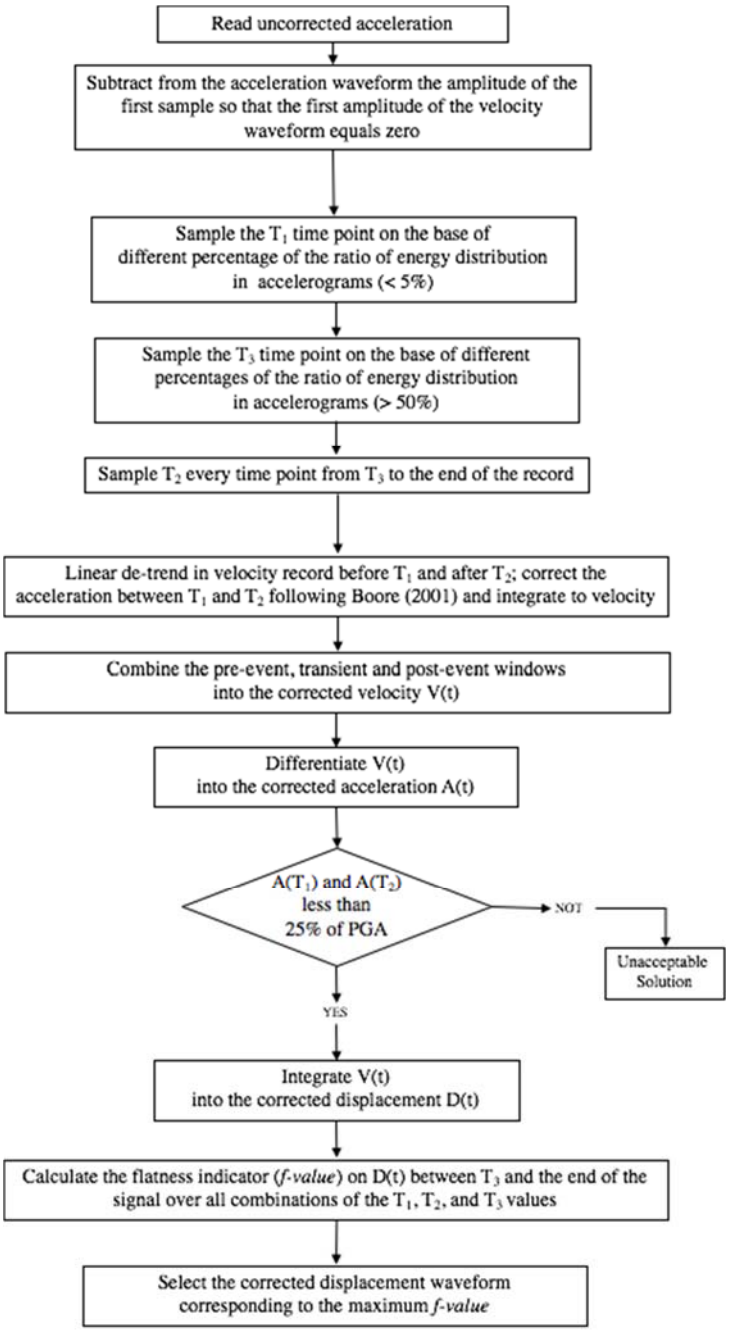

Figure 2. Flowchart of the eBASCO procedure (modified after Wu and Wu, 2007 and Chao et al., 2010).

The sampling of the correction points T_1, T_2 and T_3 makes eBASCO an automatic procedure that avoids visual inspection of the time series (Wu and Wu, 2007) or a-priori fixing of the accumulative acceleration energy thresholds (Chao et al., 2010). Even though this strategy is relatively more computationally expensive, it ensures more robust correction of the ground displacement.

3. Fling-Step Data Sources

Starting from August 2016, one of the major seismic sequences ever recorded in Italy (still ongoing) struck the central Apennine. The first shock (M_W 6.1 24th August 2016 01:36 UTC) occurred near Amatrice and was followed after two months by other two large earthquakes near Ussita (M_W 5.9 26th October 2016 19:18 UTC) and Norcia (M_W 6.5 30th October 2016 06:40 UTC). The events were recorded by about 250 temporary and permanent stations belonging to the Italian strong-motion network (*Rete Accelerometrica Nazionale*, RAN), operated by the Italian Civil Protection Department (DPC) and to the Italian seismic network (*Rete Sismica Nazionale*, RSN), operated by the *Istituto Nazionale di Geofisica e Vulcanologia* (INGV). Temporary stations of RAN and RSN were set up with the aim of monitoring the seismic sequence at higher resolution and retrieving more accurate values of the ground shaking in the near-source region (Luzi et al. 2017).

Origin times, magnitudes, hypocentral coordinates, number of recording sites, fault-to-site and epicentral distance ranges of the three mainshocks of the 2016 Central Italy sequence are listed in Table 1. The events are related to normal faulting, and are well recorded around the source (Figure 3), especially for the largest event (Norcia, M_W 6.5 30th October), and with very good quality of the recordings.

Table 1. Mainshocks of the 2016 Italian seismic sequence selected to the fling-step recovering; M_w = moment magnitude; #Sites: number of recording sites; R_{JB} = Joyner and Boore distance range; R_{epi} = epicentral distance range. Events and stations metadata are from the Engineering Strong Motion database (ESM1.0, Luzi et al. 2016; http://esm.mi.ingv, last accessed April 2018). Focal mechanisms are adopted from Pizzi et al. (2017).

Event date	Event Name	Mw	Lon. [°]	Lat. [°]	Depth [km]	#Sites	Strike [°]	Dip [°]	Rake [°]	R_{JB} [km]	R_{epi} [km]
2016-08-24 01:36:32 UTC	Amatrice	6.0	13.2340	42.6980	8.1	20	155	45	-85	1.4-26.3	8.5-45.7
2016-10-26 19:18:06 UTC	Ussita	5.9	13.1288	42.9087	7.5	28	160	40	-80	0-24.3	2.5-29.6
2016-10-30 06:40:18 UTC	Norcia	6.5	13.1107	42.8322	9.2	60	160	40	-90	0-50	4.6-66.6

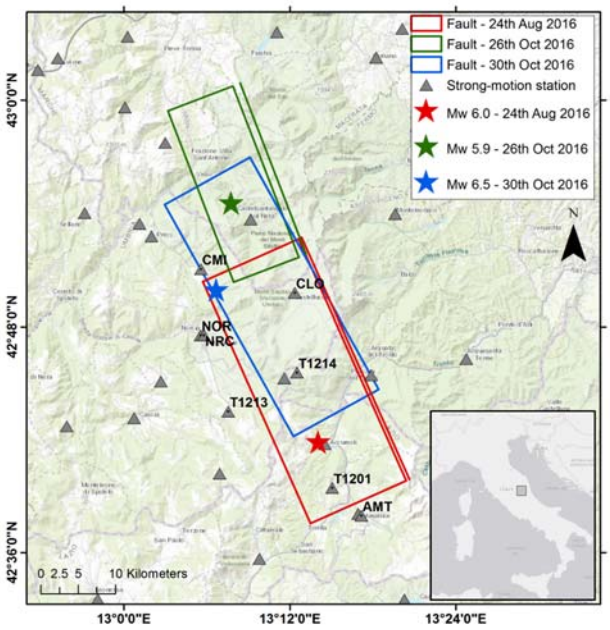

Figure 3. Geographic overview of the study area: stars are the epicenters of the Amatrice (red), Ussita (green) e Norcia (blue) earthquakes; rectangles are the surface projection of the faults. Location of strong-motion stations are also mapped (gray triangles). Events and stations metadata are from the Engineering Strong Motion database (ESM1.0, Luzi et al. 2016; http://esm.mi.ingv, last accessed April 2018). Source geometries are from Pizzi et al. (2017).

The highest strong-motion values were recorded during the Norcia earthquake (ESM, http://esm.ingv.it). The largest absolute PGAs are 869 and 782 cm/s^2 for the vertical component of T1213 and CLO stations, respectively, while the maximum PGVs are 83 cm/s (E-W component of the temporary T1201 station), 69 cm/s (Z component of the temporary station CLO), 61 cm/s (E-W component of T1213 temporary station) and 54 cm/s (E-W component of T1214 temporary station). The largest recorded absolute PGD is 23 cm (E-W component of NOR station).

The 2016 Central Italy sequence occurred along a portion of the Apennine chain characterized by high geodetic strain-rates, where a number of Global Position System (GPS) stations are operating by several public or private institutions (Cheloni et al., 2016; De Guidi et al., 2017). Concerning the Mw 6.5 30th October event (Figure 4), the largest horizontal co-seismic displacements (INGV Working Group - GPS Geodesy, 2016) were measured at the stations VETT (Mt. Vettore) and MSAN, with 38.3 cm toward north-east and 26 cm toward south-west, respectively. The largest vertical co-seismic displacements were observed for the stations ARQT, RIFP and MSAN, with a subsidence of 44.7, 26.1 and 17.1 cm, respectively. Conversely, the GPS station at Mnt. Vettore

(VETT) recorded an uplift of 5.5. cm. In addition, a detailed monitoring of the ground deformation in the surrounding of the Mt. Vettore (De Guidi et al., 2017) shows an eastward horizontal displacement around 30 cm with an upward component of motion around 3-7 cm for VTE1 and VTE2 stations (foot-wall), and westward horizontal displacement (42 and 29 cm) and subsidence (71 and 29 cm) for VTW5 and VTW4 stations (hanging-wall).

A further fling-step indicator is represented by the ground motion simulations of the Norcia event (Pizzi et al., 2017). The simulated ground motion represents a deterministic description of the long period waveforms, thus allowing correctly investigating the displacement behaviour and retrieving permanent displacement information.

4. eBASCO fling-steps versus GPS, InSAR, and simulated data

We applied eBASCO to the three mainshocks of the 2016 central Italy sequence (Table 1). About a hundreds of strong-Motion (SM) records with fault distance (R_{JB}) up to 50 km have been processed (ESUPP). In order to test the performance of the eBASCO processing scheme against nearby GPS (INGV RING Working Group, 2016) measurements and simulated ground motion (Pizzi et al., 2017), only the largest mainshock of the 2016 Central Italy sequence (Norcia earthquake; Mw6.5, 30th October) has been considered. A subset of permanent displacement values recovered by eBASCO (R_{JB} < 20 km) for the Norcia earthquake is shown in Table 2.

Table 2. Permanent displacement recovered from strong motion (SM) waveforms by means of eBASCO compared to synthetic and GPS data. Closely spaced SM and GPS are in grey (inter-distance less than 3 km); R_{epi}: epicentral distance; R_{JB}: Joyner and Boore distance; R_{rup}: distance from the rupture plane; R_x: hanging-wall distance; R_y: footwall distance.

R_{epi} [km]	R_{JB} [km]	R_{rup} [km]	R_x [km]	R_y [km]	EW_{eBASCO}	NS_{eBASCO}	UD_{eBASCO}	EW_{synth}	NS_{synth}	UD_{synth}	GPS Station	EW_{gps}	NS_{gp}
7.8	0	1.9	2.6	0	-61.7	-14.5	-85.0	-37.4	-19.9	-96.5	VTW5	-41.8	-35.3
7.7	0	2.1	2.9	0	-19.9	-32.3	-17.3	4.2	-15.6	-17.4			
11.4	0	4.5	6.2	0	-12.4	-7.2	-38.6	-9.4	5.9	-42.6	ARQT	-4.4	5.3
17.4	0	0	0	0	-1.9	15.0	-0.2	11.6	2.1	3.4			
18.6	2.2	5.7	7.3	2.2	14.9	-17.8	-3.8	-4.4	7.2	-14.2	ACCU	0.8	-0.7
8.2	2.7	9.0	12.2	0	-9.1	-0.3	2.5	-7.9	0.7	1.3			
4.6	2.8	9.1	12.4	0	-27.2	7.5	7.9	-21.8	-8.5	4.3			
9.9	3.1	9.3	12.6	0	-8.2	-3.4	1.8	-6.0	0.8	0.9	MUVI	-6.9	0.0
4.7	3.1	9.3	12.7	0	-39.7	8.1	13.6	-21.6	-8.1	4.3			
12.0	4.4	10.3	14.0	0	-15.7	-10.0	-4.7	-12.8	-7.7	2.4			
22.6	6.3	8.9	8.7	6.3	-0.4	0.9	-2.6	-2.9	3.2	-3.0			
10.5	8.8	13.4	18.4	0	-20.0	-10.0	4.7	-13.8	-5.7	1.9			
25.6	9.2	9.2	-9.0	1.6	7.5	1.6	0.1	6.9	0.7	0.3			
19.2	9.8	9.8	-9.8	0	10.0	11.5	0.6	8.9	5.3	0.5			
26.4	10.1	11.5	7.5	10.1	-0.5	1.0	2.4	-1.3	2.5	-0.3	AMAT	0.4	0.3
20.0	10.2	11.9	8.3	10.3	-2.2	-2.7	1.1	-0.6	0.1	0.4			
26.8	12.5	16.1	18.4	8.9	-3.8	-1.9	0.8	-1.6	-1.8	0.5			

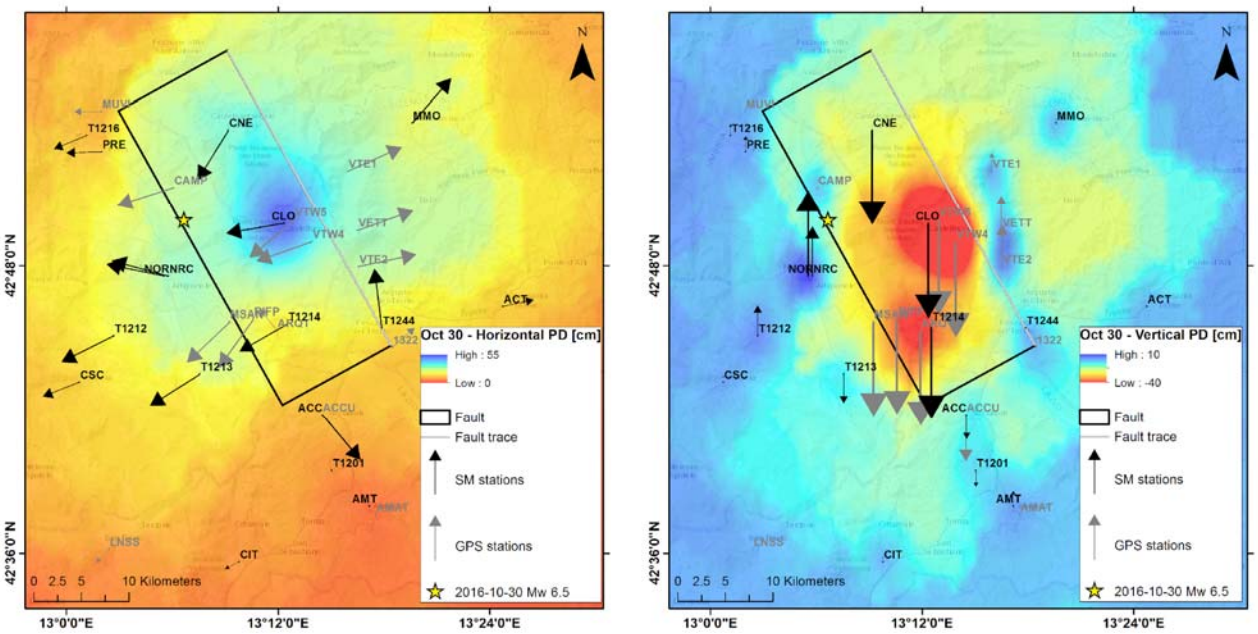

Figure 4. Interpolated map of the coseismic deformations of the M_W 6.5 30th October mainshock determined by GPS (grey arrows) (Cheloni et al., 2016; De Guidi et al., 2017) and SM stations applying the eBASCO procedure (black arrows). Left: horizontal components (vector sum); right: vertical component. Yellow star indicates the epicenter of the earthquake; black rectangle is the fault surface projection (Chiaraluce et al., 2017) and the gray line is the surface fault trace. It should be noted that the maximum length of the arrows is set to 15 cm.

The permanent displacement field (vector sum of the two horizontal components and vertical) outlined by SM data processed by eBASCO generally agree with the coseismic deformations detected by GPS instruments (Figure 4). A clear distinction between hanging-wall and foot-wall can be observed: stations located to the east of the surface fault trace (grey line in Figure 4) show a permanent displacement oriented toward north-east (MMO, ACT, VTE1, VETT, and VTE2) and positive uplift, whereas stations located over (CNE, CLO,T1214, VTW5, VTW4, and CAMP) or at the south-western edge of the fault (T1213, RIFP, and MSAN) reveal opposite sense of movement. Significant permanent displacements are also detectable at stations NOR, NRC, and T1212 (-39.7, -27.2, and -20 cm for the EW and 13.6, 7.9, and 4.7 cm for the vertical one, respectively), located beyond the western edge of the fault.

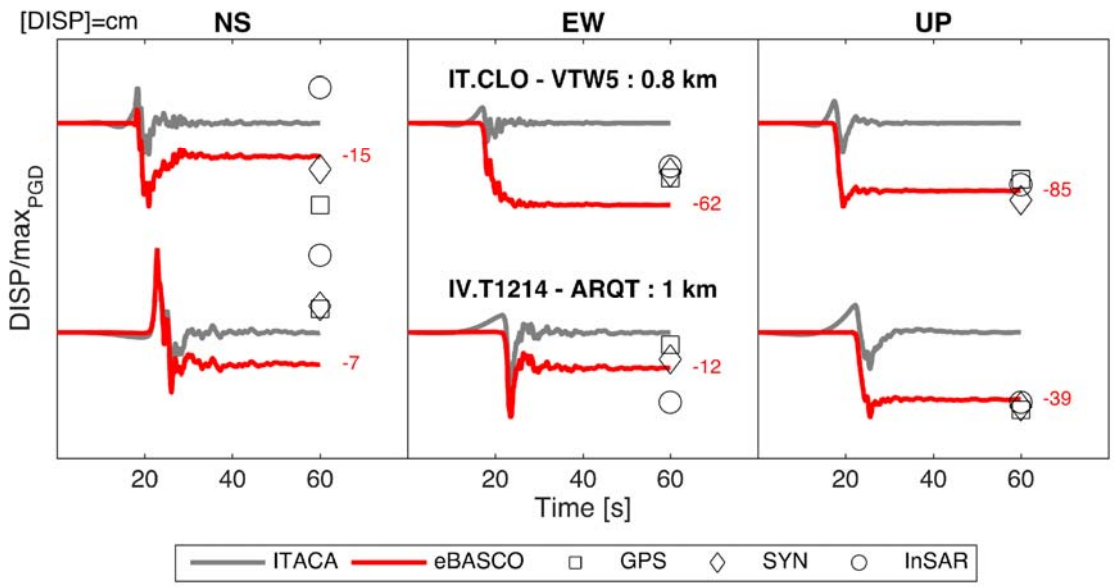

Figure 5. Comparison between ITACA (grey lines) and eBASCO (red lines) displacement waveforms (north-south [NS], east-west [EW] and vertical [UP] components plotted at the same scale). GPS (squares), synthetic (diamonds) and InSAR (circles) permanent displacements values are also plotted. The inter-distances between SM-GPS stations are also reported.

The highest levels of subsidence are for CLO and T1214 (-85 and -39 cm, respectively). In Figure 5 we compare the three components (two horizontal and vertical) displacement traces of these stations obtained by the present piecewise linear de-trend method (eBASCO) or band-pass filter (ITACA processing tool), together with a series of coseismic deformation indicators (nearby GPS, InSAR, and synthetic data). We can observe how the eBASCO time series for the vertical component feature ramp functions with negative amplitudes, matching the permanent displacements of the coseismic indicators (Figure 5). On the contrary, the ITACA traces are affected by distortion before the beginning of the strong-ground shaking characterized by positive peaks and, mostly, by oscillations around zero in the last portion of the records. The comparison can be considered satisfactory also for the east-west components (Figure 5). Regarding the north-south components, the coseismic indicators are quite scattered making it difficult to give any consideration about the eBASCO and ITACA processing performance (Figure 5).

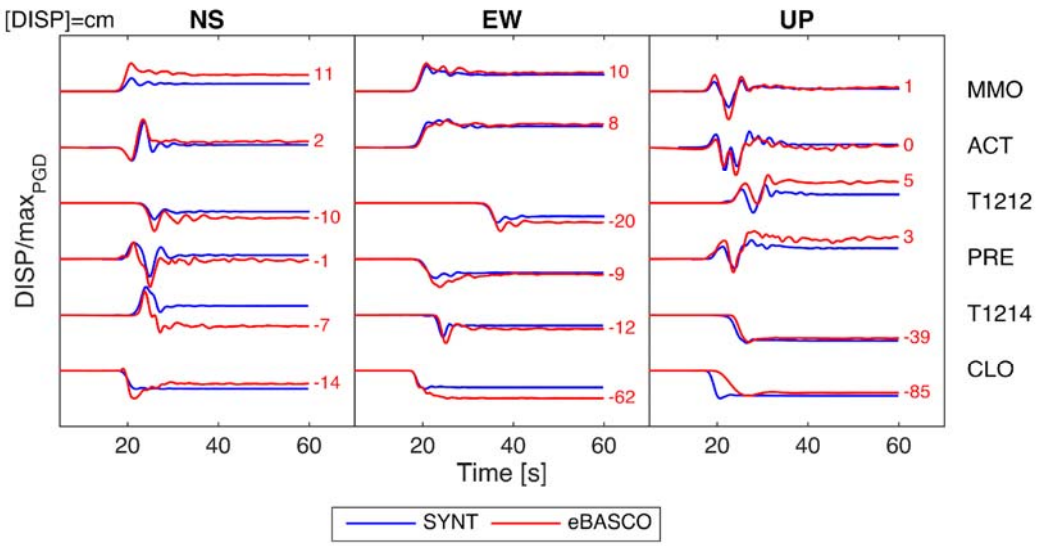

Figure 6. Comparison between synthetic (blue) and eBASCO (red) displacement waveforms (north-south [NS], east-west [EW] and vertical [UP] components plotted at the same scale) for six SM stations (MMO, ACT, T1212, PRE, T1214 and CLO). SM waveforms are low-pass filtered at 0.5Hz for graphical needs. The values next to the waveforms are static displacements in centimeters.

In Figure 6 we compare the eBASCO traces with the simulated ones for some SM stations either in hanging-wall (T1214 and CLO) or in foot-wall (MMO, ACT, T1212, and PRE). The waveforms agree very well both in terms of sign and amplitude, except in the case of the north-south component of the T1214 station and, to some extent, of the east-west component of the CLO station.

5. Fling-Step Amplitude

In this section we compare the Norcia earthquake (Mw6.5, 30th October 2016) fling-step amplitudes recovered by eBASCO with those provided by two attenuation models available for coseismic deformations (Kamai et al., 2014 in Figure 7; Burks and Baker 2016 in Figure 8).

As already pointed out, the drawback of the predictive equations for the ground permanent displacement is the paucity of near-source records containing fling. As a consequence, they are simulation based with magnitude validity range of 6.0-8.2 (Kamai et al., 2014) or derived from a dataset of simulated and recorded data with event magnitudes of 7.0-8.3 (Burks and Baker 2016). Moreover, their styles-of-faulting are reverse or strike-slip, while our data correspond to a normal fault event.

Since the majority of records comes from SM stations located in the hanging-wall, we only discuss this case. The geometrical mean horizontal component for permanent displacement larger than 1 cm attenuates with distance according to Kamai et al. (2014) and to the GPS data, whereas the vertical one tends to be over-predicted by the model (Figure 7). Indeed, the attenuation relationship is calibrated for strike-slip and reverse fault scenarios, while our data refer to a normal fault event.

The model proposed by Burks and Baker (2016) is also in agreement with the eBASCO results (Figure 8), supporting the reliability of the processing scheme. Further in-depth analysis should be done about permanent displacement recovered from SM data lower than 1 cm (see grey box in Figure 7 and 8) at distances greater than 10 km; in such cases low signal-to-noise ratios or site effects could make the use of eBASCO pointless.

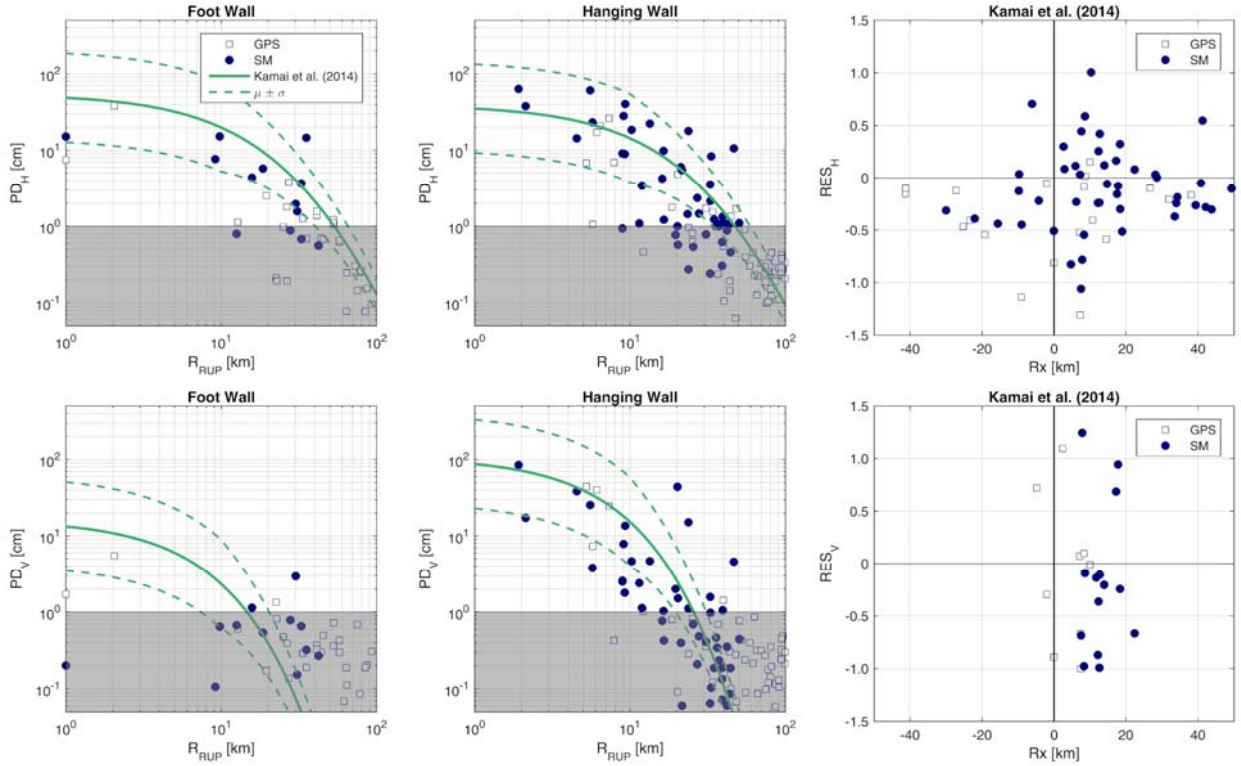

Figure 7. Permanent displacement (*PD*) from GPS (squares) and SM (circles) stations as a function of rupture distance (R_{RUP}). Kamai et al. (2014) model (green lines, horizontal *H* [a, b] and vertical *V* [c, d] components) is plotted specifically for the foot-wall and hanging-wall positions. Gray rectangle highlights the *PD* values ≤ 1 cm. Residuals (RES) as a function of the R_x distance are also reported for PD > 1 cm (positive Rx - hanging-wall, negative Rx - foot-wall?????).

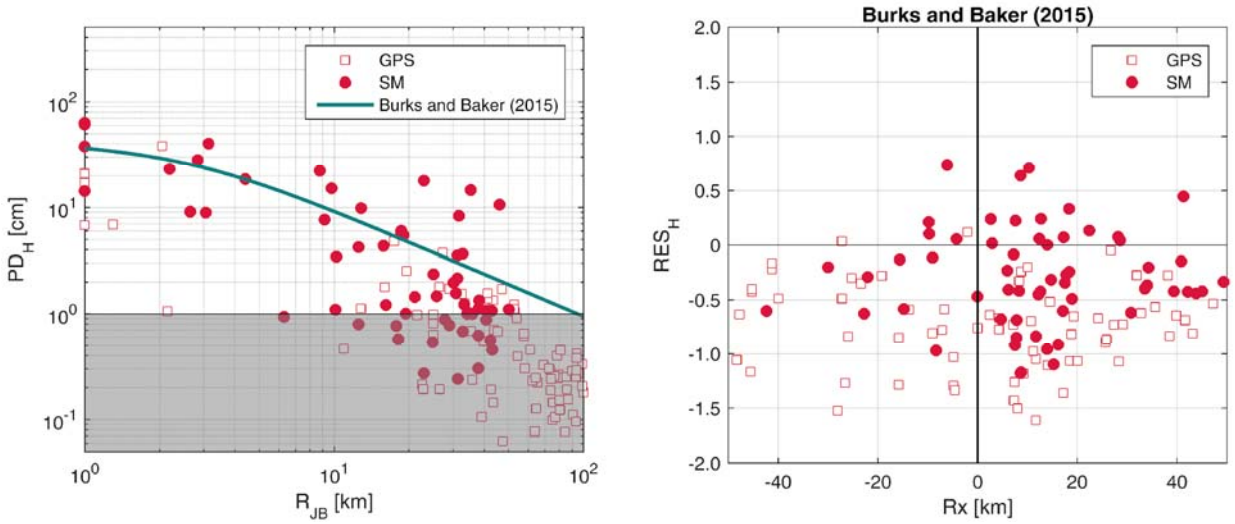

Figure 8. Horizontal permanent displacement (PD_H) amplitude as function of Joyner-Boore distance (R_{JB}) for Burks and Baker (2015) model (dark green). Gray rectangle highlights the *PD* values ≤ 1 cm. Residuals (RES) as a function of the R_x distance are also reported for PD > 1 cm.

6. eBASCO VS ITACA

6.1 Peak Parameters

In order to highlight the differences between alternative processing schemes, we compare in Figure 9 the peak ground displacement (PGD) and velocity (PGV) of the Mw 6.5, 30th October 2016 earthquake from eBASCO with those available in ITACA (http://itaca.mi.ingv.it, last accessed April 2018). As it can be noted, especially for stations located above the fault (e.g. CNE, T1214, and CLO), PGD_{eBASCO} tends to be larger than PGD_{ITACA}. This is due to the fact that the ITACA processing scheme (Paolucci et al., 2011; Pacor et al., 2011) removes the low frequency part of the signal, leading to a loss of information related to both the static (PD) and dynamic (PGD) displacement. Conversely, eBASCO applies only a piecewise baseline correction, thus preserving the low frequency content of the signal. PGVs are generally not affected by the adopted processing scheme being related to higher frequencies with respect to the displacement; for two stations located above the fault (i.e. T1214, and CLO), however, the PGVs retrieved by eBASCO are larger than that from ITACA. The same discrepancy can be observed in Figure 5; it is a clear effect of the artificial signal distortion before the beginning of the strong-ground shaking induced by the ITACA processing.

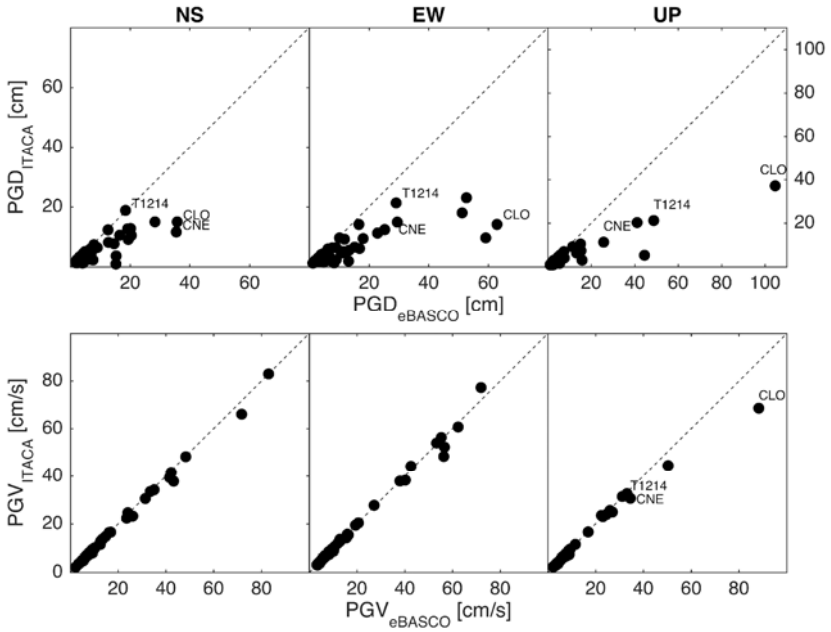

Figure 9. Peak parameters (PGD and PGV) of the M_W 6.5, 30th October earthquake retrieved by eBASCO compared to values from ITACA (http://itaca.mi.ingv, last accessed April 2018). Vertical component PGDs are plotted with a different scale compared to the two horizontal components.

6.2 Displacement Response Spectra (SD)

Performance-based seismic design has gained importance in the modern earthquake engineering and various procedures have been proposed in the last decades (Paolucci et al. 2008). A common characteristic of such methodologies is that they require a proper definition of the seismic action in terms of spectral displacement ordinates. However, recovering reliable response spectral ordinates from acceleration records up to the largest periods for engineering purposes turns out to be a challenging task (Paolucci et al. 2008). Therefore, in the following section we compare displacement response spectra obtained from ITACA and eBASCO.

At long periods the maximum relative displacement of a linear oscillator tends to the peak ground displacement (PGD). Since alternative processing methodologies provide different PGDs, one should expect that also the spectral displacement ordinates diverge at long periods. Indeed, as it can be observed in Figure 10 (upper panel), with increasing oscillator period the eBASCO response spectra provide spectral ordinates larger than ITACA. In particular, it is noted that the spectra start diverging for periods longer than 5s. As an example, Figure 10 (lower panel) shows the comparison

between SD obtained by eBASCO and ITACA for station CLO, whose displacements are consistent with the GPS and the synthetic data. It can be noted that eBASCO ordinates significantly increase between 5s and 15s, until they are more than 2 times greater than those of ITACA at larger periods. Our results contradict other studies, such as Boore (2001), who claim that the spectral ordinates with period less than about 20 s are not sensitive to the baseline corrections so that the uncertainties in response spectra due to baseline shifts should not be important at periods of interest for engineering purposes.

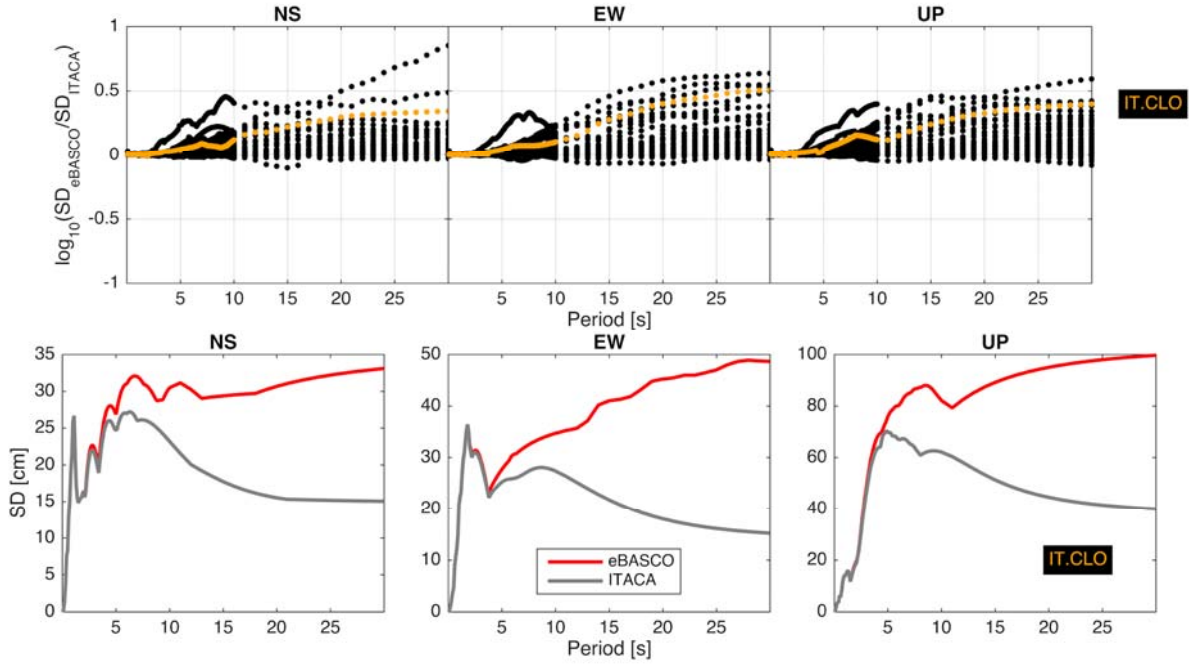

Figure 10. Upper panel: logarithm of the ratio between SD_{eBASCO} and SD_{ITACA} as a function of the period (M_W6.5, 30th October 2016) for all the stations considered. Lower panel: displacement response spectra calculated by eBASCO (red lines) for station CLO compared to those available in ITACA (grey lines). Orange circles highlight the spectral ordinates of the CLO station.

Furthermore, we analyse long-period spectral ordinates (10 and 30s) as a function of permanent displacement and PGD. Figure 11 stands out that the PDs are not correlated to the long-period ordinates. Conversely, the PGD shows a good correlation with long period response spectra, as it was expected. This is also in agreement with Faccioli et al. (2004), who stated that the ordinates at T = 10 s represent a realistic estimator of the peak ground displacement. Finally, it is pointed out how the PGD represents a lower bound of the long-period spectral ordinates in the case of ITACA.

This corroborates the hypothesis that it is necessary to better constrain the PD in order to better define the PGD as well as the importance of the processing scheme in order to obtain reliable spectral ordinates.

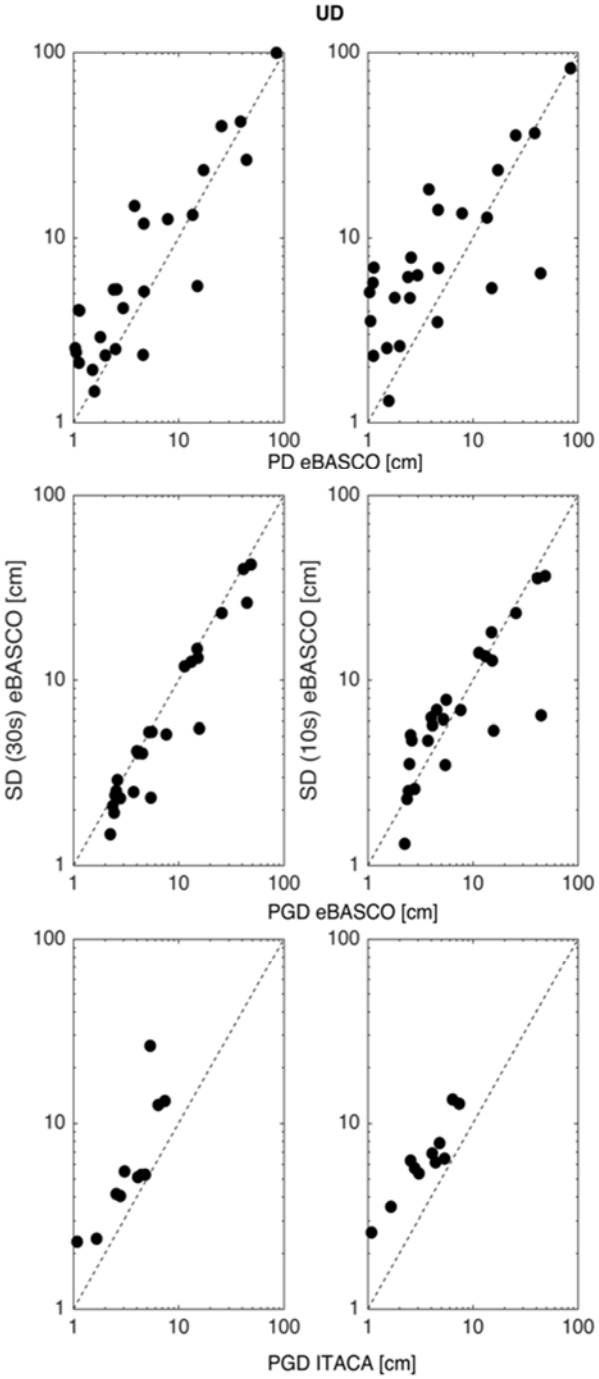

Figure 11. eBASCO spectral displacement (SD) ordinates (vertical components) at T = 30s and T = 10s as a function of PD_{eBASCO} (top), PGD_{eBASCO} (middle), and PGD_{ITACA} (bottom).

7. CONCLUSIONS

In this work, we have developed an automatic scheme, eBASCO, for piecewise base-line correction of near-source records, taken the cue from the approach proposed by Wu and Wu (2007) and successively improved by Chao et al. (2010). In particular, one of the main goals was to fine-tune a procedure that leads to a more objective criterion to evaluate coseismic displacements. Indeed, this allows avoiding the manual choice of the correction points as well as speeding up the estimation of the permanent displacement amplitude and thus the definition of the final solution. This is a key factor in populating strong motion database like ITACA (http://itaca.mi.ingv) or ESM (http://esm.ingv.it) with well qualified data, useful for earthquake engineering purposes.

The comparison between SM, GPS and synthetic data for the Mw 6.5, 30th October 2016 earthquakes highlights how the eBASCO processing is generally efficient in estimating the fling-step. Furthermore, the comparison with fling-step amplitude predictive models (Kamai et al. 2014 and Burks and Baker 2016) proves to be satisfactory, although they are calibrated on strike-slip and reverse fault scenarios with slightly larger magnitude values.

The analysis of the results has demonstrated the following:

- Generally, the PGD obtained from eBASCO results to be larger than that retrieved from ITACA. An explanation lies in the fact that the processing scheme adopted in ITACA removes the low frequency content of the signal, leading to a loss of information related to both the static (PD) and dynamic (PGD) displacement. Conversely, PGV and PGA tend to show very similar values, since they are related to higher frequencies, which are not affected by the different approaches.
- The comparison between displacement response spectra proves to be very useful for engineering purposes, especially for issues concerning performance-based seismic design.

Indeed, eBASCO and ITACA spectral ordinates start diverging from oscillating period larger than 5 s.

- Spectral ordinates at periods equal to 10 s and 30 s prove to be well correlated to the PGD, so that they can be considered as a realistic estimator of the peak ground displacement.

Further efforts will be addressed to the calibration of fling-step models (amplitude and pulse-period duration) for large-to-very-large earthquakes that account for different fault mechanism, by using the eBASCO processing scheme.

References

Ameri, G., Massa M., Bindi D., D'Alema E., Gorini A., Luzi L., Marzorati S., Pacor F., Paolucci R., Puglia R., Smerzini C. (2009). The 6 April 2009 Mw 6.3 L'Aquila (Central Italy) Earthquake: Strong-motion Observations. Seismological Research Letters 80, 951–966.

Avallone, A., Latorre, D., Serpelloni, E., Cavaliere, A., Herrero, A., Cecere, G., D'Agostino, N., D'Ambrosio, C., Devoti, R., Giuliani, R., Mattone, M., Calcaterra, S., Gambino, P., Abruzzese, L., Cardinale, V., Castagnozzi, A., De Luca, G., Falco, L., Memmolo, A., Migliari, F., Minichiello, F., Moschillo, R., Massucci, A., Zarrili, L., & Selvaggi, G. (2016). Coseismic displacement waveforms for the 2016 August 24 Mw 6.0 Amatrice earthquake (central Italy) carried out from High-Rate GPS data. Annals of Geophysics, 59. doi:http://dx.doi.org/10.4401/ag-7275

L. Chiaraluce, R. Di Stefano, E. Tinti, L. Scognamiglio, M. Michele, E. Casarotti, M. Cattaneo, P. De Gori, C. Chiarabba, G. Monachesi, A. Lombardi, L. Valoroso, D. Latorre, S. Marzorati (2017). The 2016 Central Italy Seismic Sequence: A First Look at the Mainshocks, Aftershocks, and Source Models. Seismological Society of America, Volume 88, Number 3. DOI: 10.1785/0220160221

Cheloni D, Serpelloni E, Devoti R, D'Agostino N, Pietrantonio G, Riguzzi F, Anzidei M, Avallone A, Cavaliere A, Cecere G, D'Ambrosio C, Esposito A, Falco L, Galvani A, Selvaggi G, Sepe V, Calcaterra S, Giuliani R, Mattone M, Gambino P, Abruzzese L, Cardinale V, Castagnozzi A, De Luca G, Massucci A, Memmolo A, Migliari F, Minichiello F, and Zarrilli L. (2016). GPS observations of coseismic deformation following the 2016, August 24, Mw6 Amatrice earthquake (central Italy): data, analysis and preliminary fault model. Annals of Geophysics, 59, Fast Track 5, 1–8. doi:10.4401/ag-7269

INGV Working Group “GPS Geodesy (GPS data and data analysis center)”, 2016a. Preliminary co-seismic displacements for the August 24, 2016 ML6, Amatrice (central Italy) earthquake from the analysis of continuous GPS stations, DOI: 10.5281/zenodo.61355.

INGV Working Group “GPS Geodesy (GPS data and data analysis center)", 2016b. Preliminary co-seismic displacements for the October 26 (Mw5.9) and October 30 (Mw6.5) central Italy earthquakes from the analysis of GPS stations. DOI: http://doi.org/10.5281/zenodo.167959

Luzi L, Puglia R, Russo E & ORFEUS WG5 (2016). Engineering Strong Motion Database, version 1.0. Istituto Nazionale di Geofisica e Vulcanologia, Observatories & Research Facilities for European Seismology. doi: 10.13127/ESM

Akkar S., Sandıkkaya M.A., Şenyurt M., Azari Sisi A., Ay B.Ö., Traversa P., Douglas J., Cotton F., Luzi L., Hernandez B., Godey S. (2013). Reference database for seismic ground-motion in Europe (RESORCE), Bulletin of Earthquake Engineering, DOI: 10.1007/s10518-013-9506-8, in press, http://link.springer.com/article/10.1007/s10518-013-9506-8

Boore, D. M. (2005). On pads and filters: Processing strong-motion data, Bull. Seismol. Soc. Am. 95, 745–750.

Boore, D. M., and S. Akkar (2003). Effect of causal and acausal filters on elastic and inelastic response spectra, Earthq. Eng. Struct. Dynam. 32, 1729–1748.

Boore DM, BOMMER JJ (2005) Processing of strong-motion accelerograms: needs, options and consequences. Soil Dynamics and Earthquake Engineering 25:93–115. doi: 10.1016/j.soildyn.2004.10.007

Douglas, J. and Boore D. M. (2011). High-frequency filtering of strong-motion records, Bull earthquake Eng, 9(2), 395–409, doi:10.1007/s10518-010-9208-4.

Ancheta TD, Darragh RB, Stewart JP, Seyhan E, Silva WJ, Chiou BSJ, Wooddell KE, Graves RW, Kottke AR, Boore DM, Kishida T, Donahue JR (2014) NGA-West2 database. Earthq Spectra 30(3):989–1005

Graves R.W. (2004) - Processing Issues for near source Strong Motion Recordings: http://www.cosmos- eq.org/events/wkshop_records_processing/papers/Graves.pdf.

Wang, R., Schurr, B., Milkereit, C., Shao, Z. & Jin, M. (2011) An Improved Automatic Scheme for Empirical Baseline Correction of Digital Strong-Motion Records. Bulletin of the Seismological Society of America 101, 2029–2044.

Burks L.S. and Baker J. W. (2016). A predictive model for fling-step in near-fault ground motions based on recordings and simulations. Soil Dynamics and Earthquake Engineering. Vol. 80, 119-126. https://doi.org/10.1016/j.soildyn.2015.10.010

Kamai R., Abrahamson N., Gaves R. (2014). Adding Fling Effects to Processed Ground-Motion Time Histories. Bulletin of the Seismological Society of America, Vol. 104, No. 4, pp. 1914–1929, doi: 10.1785/0120130272

Kalkan E, Kunnath SK (2006) Effects of Fling Step and Forward Directivity on Seismic Response of Buildings. Earthquake Spectra 22:367–390. doi: 10.1193/1.2192560

Mavroeidis GP, Papageorgiou AS (2003) A Mathematical Representation of Near-Fault Ground Motions. Bulletin of the Seismological Society of America 93:1099–1131.

Bray JD, Rodriguez-Marek A (2004) Characterization of forward-directivity ground motions in the near-fault region. Soil Dynamics and Earthquake Engineering 24:815–828. doi: 10.1016/j.soildyn.2004.05.001

Somerville, P.G., 2005. Engineering characterization of near fault ground motions. NZSEE Conference, (1), pp.1–8.

Somerville, P.G. (2002). Characterizing near fault ground motion for the design and evaluation of bridges. Proceedings of the Third National Conference and Workshop on Bridges and Highways, Portland, Oregon, April 29 – May 1, 2002

Kalkan E, Kunnath SK (2006) Effects of Fling Step and Forward Directivity on Seismic Response of Buildings. Earthquake Spectra 22:367–390. doi: 10.1193/1.2192560

Akkar S, Boore DM (2009) On Baseline Corrections and Uncertainty in Response Spectra for Baseline Variations Commonly Encountered in Digital Accelerograph Records. Bulletin of the Seismological Society of America 99:1671–1690. doi: 10.1785/0120080206

Boore, D.M., 2001. Effect of baseline corrections on displacements and response spectra for several recordings of the 1999 Chi-Chi, Taiwan, earthquake. Bulletin of the Seismological Society of America.

R. Puglia, E. Russo, L. Luzi, M. D'Amico, C. Felicetta, F. Pacor, G. Lanzano (2018) Bull Earthquake Eng 2018 Puglia. Bull Earthquake Eng 1–11. doi: 10.1007/s10518-017-0299-z

Graves, Robert, W., 2004. Processing Issues for Near Source Strong Motion Recordings. Presented. Workshop on Strong-Motion Recording Processing, Consortium of Organizations for Strong-Motion Observation Systems, pp.193–201. Available at: http://www.cosmos-eq.org/events/wkshop_records_processing/papers/Graves.pdf.

Abrahamson NA. Velocity pulses in near-fault ground motions. In: Proceedings of the UC Berkeley - CUREE Symposium in Honor of Ray Clough and Joseph Penzien. Berkeley, California; 2002, p. 40–1.

Wang R, Schurr B, Milkereit C, Zhigang S, and Mingpei J (2011) An Improved Automatic Scheme for Empirical Baseline Correction of Digital Strong-Motion Records. Bulletin of the Seismological Society of America 101:2029–2044. doi: 10.1785/0120110039

Chen SM, Loh CH (2007) Estimating Permanent Ground Displacement from Near-Fault Strong-Motion Accelerograms. Bulletin of the Seismological Society of America 97:63–75. doi: 10.1785/0120060060

Wu, Y.M. & Wu, C.F., 2007. Approximate recovery of coseismic deformation from Taiwan strong-motion records. Journal of Seismology, 11(2), pp.159–170

Boore, D.M., Stephens, C.D. & Joyner, W.B., 2002. Comments on baseline correction of digital strong-motion data: Examples from the 1999 Hector Mine, California, earthquake. Bulletin of the Seismological Society of America, 92(4), pp.1543–1560.

Graizer, G.M., 1979. Determination of the true ground displacement by using strong motion records. Izvestiya Physics of the Solid Earth, 15, pp.875–886.

Iwan WD, Moser MA, Peng CY (1985) Some observations on strong-motion earthquake measurement using a digital accelerograph. Bull Seismol Soc Am 75:1225–1246

Graves, Robert, W., 2004. Processing Issues for Near Source Strong Motion Recordings. Presented. Workshop on Strong-Motion Recording Processing, Consortium of Organizations for Strong-Motion Observation Systems, pp.193–201. Available at: http://www.cosmos-eq.org/events/wkshop_records_processing/papers/Graves.pdf.

Chen, S.M. & Loh, C.H., 2007. Estimating permanent ground displacement from near-fault strong-motion accelerograms. Bulletin of the Seismological Society of America, 97(1 B), pp.63–75.

Chao, W.A., Wu, Y.M. & Zhao, L., 2010. An automatic scheme for baseline correction of strong-motion records in coseismic deformation determination. Journal of Seismology, 14(3), pp.495– 504.

Giorgio De Guidi1,2, Alessia Vecchio1, Fabio Brighenti1, Riccardo Caputo3,4,5, Francesco Carnemolla1, Adriano Di Pietro1, Marco Lupo1, Massimiliano Maggini3,5, Salvatore Marchese1,

Danilo Messina1, Carmelo Monaco1,2, and Salvatore Naso1 (2018) Brief communication: Co-seismic displacement on 26 and 30 October 2016 (Mw = 5.9 and 6.5) – earthquakes in Central Italy from the analysis of a local GNSS network Nat. Hazards Earth Syst. Sci., 17, 1885–1892, 2017 https://doi.org/10.5194/nhess-17-1885-2017

Pizzi A, Di Domenica A, Gallovic F, et al (2017) Fault Segmentation as Constraint to the Occurrence of the Main Shocks of the 2016 Central Italy Seismic Sequence. Tectonics 36:2370–2387. doi: 10.1785/0120070111